Reliability of Liquid Crystals in Space Photonics

6 authors, including:

Eva Otón
Nikon and Essilor International Joint Researc...
30 PUBLICATIONS   47 CITATIONS

SEE PROFILE

Demetrio López Molina
Alter Technology
2 PUBLICATIONS   0 CITATIONS

SEE PROFILE

José M. Otón
Universidad Politécnica de Madrid
211 PUBLICATIONS   1,117 CITATIONS

SEE PROFILE

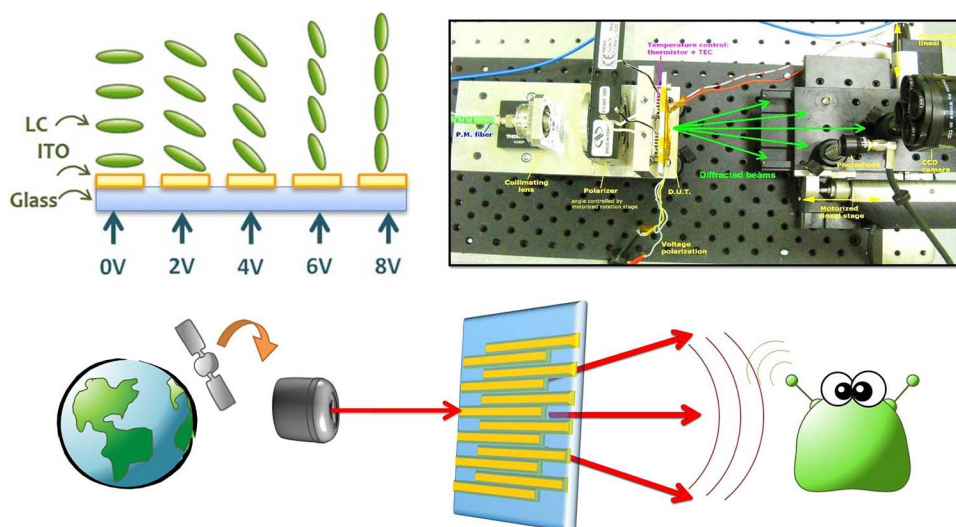Morten Andreas Geday
Universidad Politécnica de Madrid
85 PUBLICATIONS   461 CITATIONS

SEE PROFILE

Reliability of Liquid Crystals in Space Photonics

Eva Otón
Javier Pérez-Fernández
Demetrio López-Molina
Xabier Quintana
José M. Otón
Morten A. Geday

Reliability of Liquid Crystals in Space Photonics

Eva Otón,[1] **Javier Pérez-Fernández,**[2] **Demetrio López-Molina,**[2]
Xabier Quintana,[1] **José M. Otón,**[1] **and Morten A. Geday**[1]

[1]CEMDATIC, ETSI Telecomunicación, Universidad Politécnica de Madrid, 28040 Madrid, Spain
[2]Alter Technology Group Spain, 28760 Tres Cantos, Spain

Abstract: Passive liquid crystal (LC) devices are becoming an interesting alternative for the manufacturing of photonic devices in spatial applications. These devices feature a number of advantages in this environment, the lack of movable parts, and of exposed electronics being among the most outstanding ones. Nevertheless, the LC material itself must demonstrate its endurance under the harsh conditions of space missions, including launch and, perhaps, landing. In this paper, we present the environmental testing of an LC device for space applications. A number of LC based beam steering devices were manufactured, characterized, and tested in a series of destructive and nondestructive tests defined by the European Space Agency (ESA). The purpose was to evaluate the behavior and possible degradation of the LC response in simulated space environments. Device fabrication and testing was done within an ESA-funded project, whose purpose was the design, manufacturing, and characterization of adaptive optical elements, as well as the execution of qualification tests on the devices in space-simulated conditions.

Index Terms: Liquid crystal, photonic device, space optics, damage test, space-simulated condition.

1. Introduction

Liquid crystal (LC) devices are increasingly being used in non-display applications to manufacture low-cost, light-weight small devices that can be driven by low-voltage electronics. Avoiding the use of movable parts or mechanical elements is particularly desirable in certain circumstances, e.g., space applications [1]–[4].

Non-display photonic devices based on LCs can be either phase-modulation or amplitude-modulation devices [5]. A number of LC photonic devices induces phase delays between different positions of the wavefront resulting in spatial light modulators (SLM) [6], [7]. SLMs have been used in many scenarios, e.g., spatial filters, holograms [8], light-path compensators, tunable lenses [9], or beam steerers [10], [11].

Commercial and experimental LC spatial filters and holograms are chiefly based on active thin film transistor (TFT) microdisplays or on high-density microdisplays on silicon backplanes aka liquid crystal on silicon (LCoS) displays. Lenses and beam steerers, on the other hand,
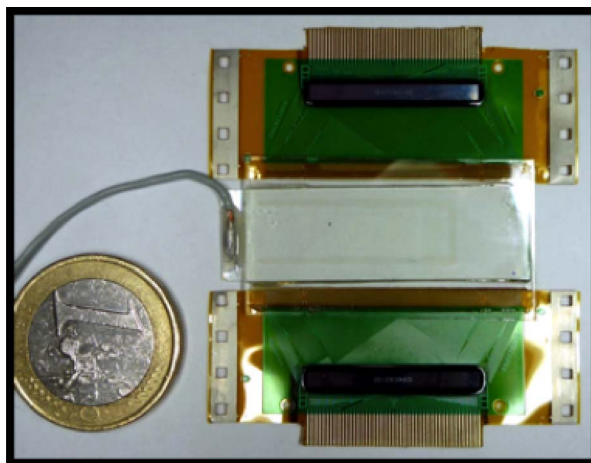
Fig. 1. Manufactured beam steerers. The active area of ca. 5 mm × 7 mm is located at the center of the glass plates. The chip-on-flex electronics are the two horizontal black bars above and below the LC cell.

may be manufactured in a number of different styles, including passive-driven and monopixel solutions. The behavior of such devices depends on the conducting surfaces, alignment conditions, and LC material; thus, a large number of variables are available for tuning these devices to specific applications [12]–[14].

In this work, we present the results obtained within the context of the ESA-funded project Programmable Optoelectronic Adaptive Element (AO/1-5476/07/NL/EM). The ESA-POE Beam Steering device is a liquid crystal based tunable blaze grating for space applications, i.e., a 1D SLM. A laser beam can be steered certain angles, step-by-step, depending on the grating period. The main goal of the work was to ascertain the suitability of LC photonic devices for spatial photonic devices. The qualification is done by undertaking several destructive and non-destructive tests defined by ESA.

The device manufacturing process was done keeping in mind the conditions and environment the device has to undergo in a space mission: extreme temperature variations, pressure variation, vibrations, and high-energy ionizing radiation. Thus, high-density electronic structures, such as thin film transistors or LCoS technology, were avoided in the active area. Instead, the pixel addressing is done using passive transparent indium-tin oxide (ITO) coated onto glass plates, controlled by electronics situated aside the active area. In doing so, only the ITO tracks, the LC, and the supporting substrate will be exposed to external radiation. The remaining electronics can be easily shielded, and system damage induced by radiation becomes largely alleviated.

2. Experimental

2.1. Cell Design and Construction

The manufactured photonic device is a beam steerer consisting of two 1.1 mm thick ITO-coated glass substrates (PräzisionsGlas&OptikCEC015S, Germany) assembled in a sandwich-like cell and filled with liquid crystal (see Fig. 1). One of the glass substrates is pixelated with 768 high-density interleaved transparent ITO electrodes. The counter electrode is a continuous ITO backplane. Two chip-on-flex mounted display drivers (SSD1783BU2-COF, Solomon Systech, USA) are employed for addressing the 2 × 384 interlaced electrodes in the 5.376 mm × 7 mm active area. The high-density interconnections between the flex circuit and the ITO electrodes were achieved using an Anisotropic Conductive Adhesive (ACA, Hitachi Chemical Europe).

Electrodes can be independently driven. Applying increasing voltages between top and bottom electrodes, the LC switches on in a stepped forward profile, i.e. a stepped refractive index profile is obtained (see Fig. 2).
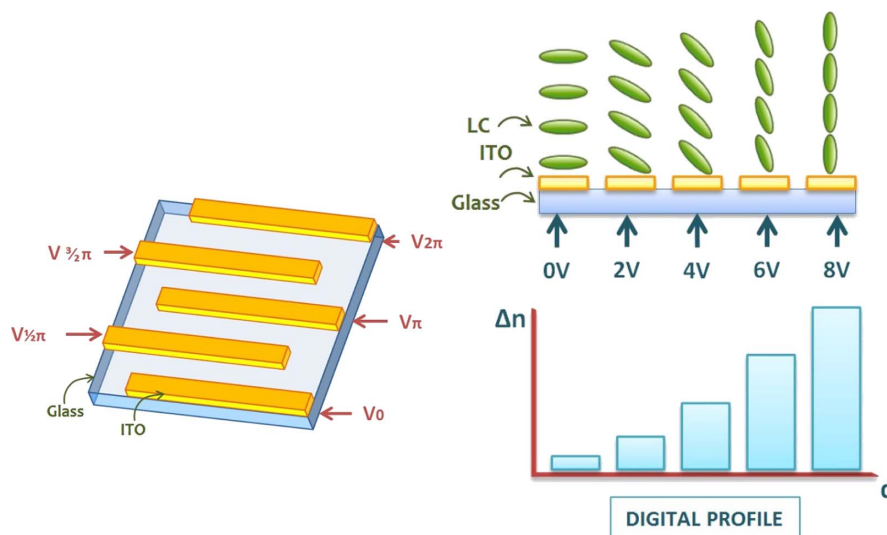
Fig. 2. Beam steerer design. (Left) Different voltages are applied on each electrode causing progressive LC switching on the electrode sequence (top right). (Bottom right) Obtained refractive index profile.

An optimization of the fine resolution photolithographic process led to two interleaved combs with approximately 5 mm long, 5.5 μm wide pixels in a 7 μm pitch. The diffraction efficiency was estimated. Four ideal (i.e., sharp) refractive index steps correspond to a theoretical diffraction efficiency of 82%. The LC response, however, is somewhat smoothened by fringing effects on the electrode edges. To what extent the smooth behavior of the LC may improve or worsen the response of the device ultimately depends on the nature of the devices i.e. the viscosity of the liquid crystal, the thickness of the cell, the fill factor, and the nature of the alignment surfaces. In either case, the main aim of this work was monitoring LC degradation and not cell optimization.

The most suitable liquid crystals for this application are high birefringence LCs, so that thinner cells can be produced, whereby parasitic diffraction caused by fringing can be reduced. Two kinds of LCs with acceptable birefringence were tested: a vertically aligned nematic (VAN, Merck LC-7029, $\Delta n = 0.17$) and a nematic liquid crystal for homogeneous alignment with a low freezing point (Merck MDA-98, $\Delta n = 0.266$). VAN devices have the additional advantage that having less UV absorption in their relaxed vertical state, thus increasing their tolerance against UV damage [15].

Both organic and inorganic layers can be used as alignment layers for high birefringence liquid crystals. In spatial environments, inorganic alignments like silicon oxides shall be preferred if feasible, since they are much more resilient to photochemical degradation, and susceptible to permanent damage upon freezing of the LC. Inorganic alignments, obtained by oblique evaporation, were first tested in VAN liquid crystals [16]. SiOx was found not to align high birefringence materials, and thus it was decided to employ e-gun deposited silica, SiO_2. However during the assembly of the cell, SiO_2 proved to be extremely sensitive to adsorption of organic materials, altering the VAN liquid crystal alignment. The outgassing of the gasket material, that glues the cell together during the curing process, is thought to be the main source of organic contamination [17].

Homogenous liquid crystal MDA-98 was tested with polyimide as alignment layer. In this case a perfectly homogenous alignment was obtained, so MDA-98 was chosen over MLC-7029. Employing an organic alignment layer, as mentioned above, could be a disadvantage for these devices in space environment conditions [18]. Nevertheless, including organic alignment layers would provide interesting results within the scope of this work.

External electronic driving was achieved with chip-on-flex (COF) technology, as it was considered the most suitable solution being an ideal compromise between two alternative solutions: chip-on-glass and PCB mounted drivers. COF technology reduces the problem of differential thermal dilatation that would jeopardize the interconnection in rigid silicon driver chips mounted directly on glass. The other alternative, i.e., a PCB mounted driver, would require a very high resolution PCB along with the high-resolution ITO electrodes.

Thus, COF not only features compact design, space compatibility and mechanical stability, but also the technology process was achievable in a manufacturing series and the chips were affordable. The possibility of distancing the chip from the active area of the device would facilitate any necessary shielding of the electronics.

Transmission measurements were performed in a setup consisting of a He-Ne laser with a maximum output peak of 5 mW at 543 nm, a polarizer and holder where the cell is placed, photodetector and waveform generator Stanford Research Systems DS345. Response time measurements were carried out in isothermal conditions in a Mettler FP900, containing a FP90 processor and hot plate FP82HT, where the cell is placed. The cell can be observed under a microscope Nikon Optiphot2-Pol between crossed polarizers and transmitted light is detected in a high sensitivity photomultiplier Hamamatsu HS783-01. The response is analyzed in a Tektronik TDS 714L digital oscilloscope, which is connected to a PC and driven by a LabView application [19]. Liquid crystal orientation profiles may be imaged between crossed polarizers at $\pm 45°$.

2.2. Tests for Space Simulated Conditions

Six different destructive and non-destructive tests were executed on the beam steering devices. The experiments were done in conformity with ESA specifications. The aim is to study the devices behavior and their performance when exposed to the environmental conditions of a space mission.

Eight samples were manufactured for the analysis. Six samples underwent the six tests, one for each test, one sample underwent the six tests and one sample was kept off as a reference. All cells were characterized in a non-destructive analysis before the destructive tests. Non-destructive analysis consisted of a visual inspection of the cell transparency in active area and an internal inspection under microscope, between crossed polarizers. Response times, optical power diffraction efficiency and transmission levels were measured before and after every test. The performed tests were

- total ionizing dose radiation test;
- displacement damage radiation test;
- optical power damage test;
- non-operational thermal cycling test;
- thermal vacuum test;
- vibration test.

Samples were measured in an optical test bench (see Fig. 3) and compared to the reference sample and their previous performance.

3. Results

The characterization of the devices comprised two steps. The first step aims to evaluate the liquid crystal device behavior, including:

- creating a diffraction pattern when the laser beam passes through the liquid crystal cell;
- measuring the transmission change of the laser beam when modifying applied voltages;
- measuring maximum achieved deflection angle and efficiency of first-order diffraction;
- measuring response times.

The second characterization step is a series of tests to evaluate the behavior and possible degradation of the LC response in space simulated environments. The optical power efficiency, response times and transmission changes (in working conditions) after every test were measured.
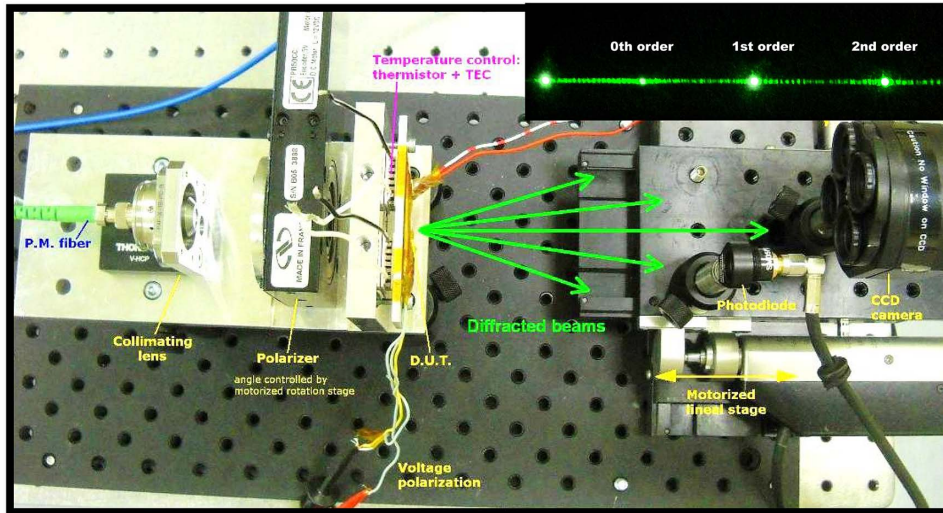
Fig. 3. Optical bench for measuring samples after tests. (Inset) Diffraction pattern of the device working as a binary grating. Note that the two first order diffraction points (1 and −1) are saturated in the picture.
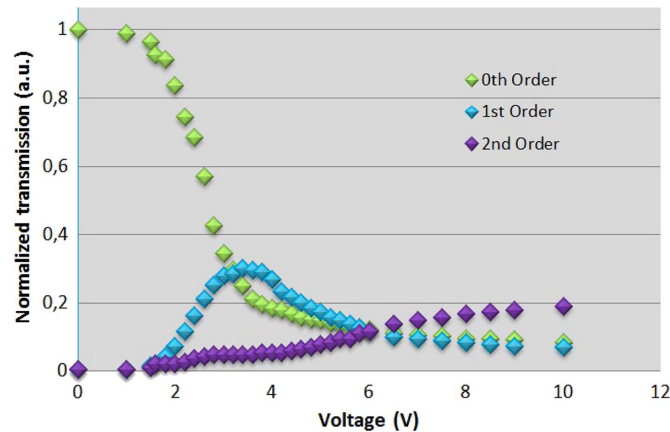

Fig. 4. Transmission–voltage measurements for zeroth, first, and second orders. Note that first order is halved since two identical maxima (+1 and −1) are obtained in binary gratings.

3.1. Electrooptical Measurements

Cells were placed in the transmission measurement setup; applying a series of voltages, different diffraction patterns are observed. All transmission measurements were carried out with cells working as binary gratings, i.e., pixels switched on and off alternatively.

The optimal working voltage is obtained when the phase delay equals π, since the 1st order reaches its maximum transmission and the zeroth order transmission tends to zero. Fig. 3 shows an example of optimal voltage: 0th order almost disappeared and beam power is deflected to the two 1st orders.

Fig. 4 shows the transmission levels for zeroth, first and second orders when increasing the device voltage for one of the test devices. Transmission levels vary when increasing voltage. 0th order decreases to its minimum while 1st order increases to its maximum. 2nd order remains approximately constant over the whole voltage range.

TABLE I

Total ionizing dose radiation test steps

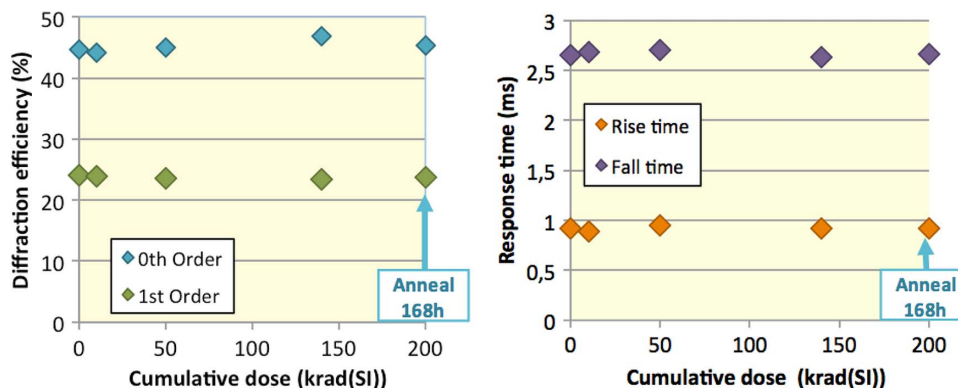|	Dose (krad(SI))	Rate (rad(SI)/h)	Exposure time (h)
Step 1	10	550	18
Step 2	40	550	73
Step 3	90	550	163

Fig. 5. Optical power diffraction efficiency and response times after cumulating ionizing radiation doses.

The performance of the manufactured devices is (in average) as follows: optimal working voltages is 3.8 ± 0.2 V, 1st order efficiency is 28% and maximum deflection angle (for binary grating) is $2.17°$.

3.2. Space Simulated Conditions Tests

3.2.1. Total Ionizing Dose Radiation Test (Gamma)

Radiation tests raised more concern than any other test. Given that final prototype samples are made with organic components, liquid crystal and possibly polyimide as alignment layer, they could be damaged when exposed to certain radiation levels. Total ionizing dose gamma radiation test was carried out in the Cobalt-60 facilities of CIEMAT (Centro de Investigaciones Energéticas, Medioambientales y Tecnológicas) in Madrid, Spain, following the steps described in Table I.

Samples underwent the total ionizing dose radiation tests up to a cumulative dose of 140 krad (SI) and a later step of 168 hours of annealing. Power diffraction efficiency and response times were measured after each step as shown in Fig. 5. No significant deviations were found when compared to the initial values or the reference device. No darkening of the glass substrates was observed either.

3.2.2. Displacement Damage Radiation Test (H^+)

Displacement damage protons radiation test was performed using ESA specifications shown in Table II. Radiation sessions were performed at CRC (Centre de Recherches du Cyclotron) of Université Catholique de Louvain (UCL), located in Louvain-la-Neuve, Belgium. Samples were measured after each displacement damage step up to a cumulative fluence level of 3×10^{11} p/cm^2, and after 168 h of annealing as well. Both power diffraction efficiency and response times (see Fig. 6) did not show substantial variations from the initial measured values or compared to the reference device.

TABLE II

Displacement damage radiation test steps

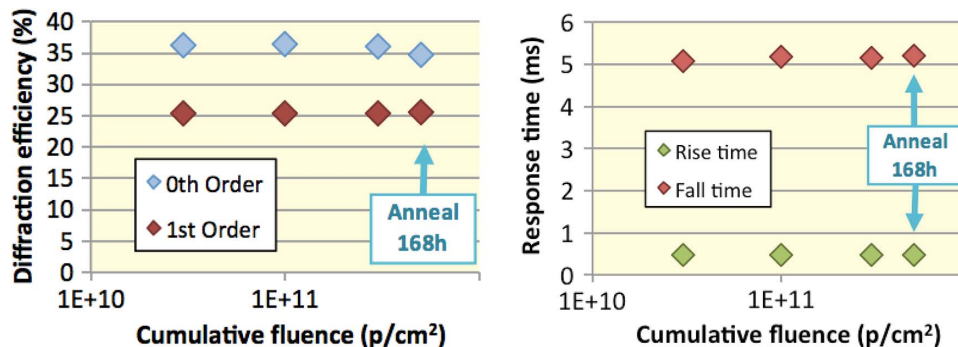|	Cum.fluence (p/cm^2)	Flux (p/cm^2/s)	Energy (MeV)	Exposure time (s)
Step 1	3×10^{10}	2×10^8	60	150
Step 2	1×10^{11}	2×10^8	60	350
Step 3	3×10^{11}	2×10^8	60	1000

Fig. 6. Optical power diffraction efficiency and response times after displacement radiation steps.
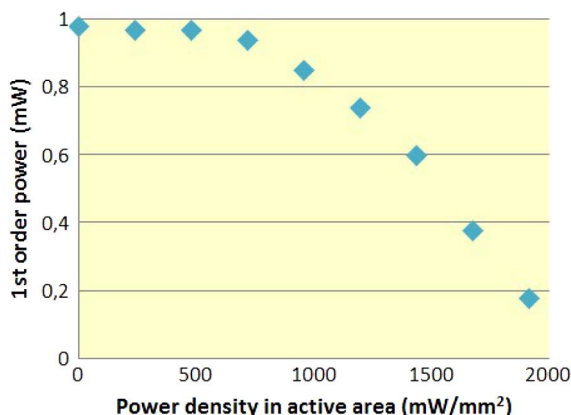

Fig. 7. Measured 1st order optical power versus power density in active area.

3.2.3. Optical Power Damage Test

Optical power damage test was performed applying a high power laser beam to the active area of the devices while working to test samples resistance to high power incident light beams. The laser is a Keopsys fiber laser KPS-BT-TYFA-1100-200-FA working at 1080 nm with a maximum output power of 20 W. The incident laser beam (2 mm diameter) interacts with the liquid crystal modifying its behavior. Power diffraction efficiency of the 1st order was measured while increasing incident laser power with a Newport CCD beam profiler.

First order optical power decreased when increasing the incident laser beam power in the active area. For power densities higher than 2000 mW/mm^2 in the active area (laser power set at 7 W), 1st order could be considered extinct (Fig. 7).

The temperature of the active area was measured with a thermal camera. Temperature increased progressively when increasing laser power density on the samples, reaching liquid

TABLE III

Thermal cycle test steps

	T_{MAX} (ºC)	T_{MIN} (ºC)	Dwell time (min)	Rate (ºC/min)	Number of cycles
Step 1	+80	-20	10	5	25
Step 2	+80	-20	10	5	75
Step 3	+80	-40	10	5	25

TABLE IV

Thermal vacuum test steps

	T_{MAX} (ºC)	T_{MIN} (ºC)	Dwell time (min)	Rate (ºC/min)	Vacuum (mbar)	# of cycles
Step	+50	+5	120	<20	<10^{-5}	5

crystal clearing point 109 °C at 2150 mW/mm^2 in the active area. At temperatures of 180 °C and higher (2900 mW/mm^2), samples began to show damage and the substrates eventually cracked.

3.2.4. Non-Operational Destructive Tests

The three non-destructive tests consisted of: non-operational thermal test, thermal vacuum test (operational) and vibration cycle tests. Thermal cycle tests resulted in a slight increase in response times although the optical diffraction efficiency remained unaltered.

Non-operational thermal cycling tests consisted of a number of thermal cycles being applied to samples, as seen in Table III.

The tested samples were measured after each set of cycles and they showed no major deviations upon completion of the cycles. Both optical power diffraction efficiency and rise times did not show any variation, however, fall times tended to increase slightly, i.e., about 8%, with additional thermal cycles.

The thermal vacuum test was performed while the device was in operation. This test was performed in a custom thermal vacuum system, equipped with a vacuum chamber, a turbomolecular pump and a climatic chamber.

The thermal cycles were performed as described in Table IV. Measuring devices behavior during the tests was performed with an optical system in the chamber: incident light enters the chamber through an optical fiber and refracted light is measured from a borosilicate glass viewport. The optical power efficiency remained approximately constant during the whole set of measurements. Response times were also measured during the thermal cycles and the tested cells showed slight increasing rise and fall times after thermal vacuum tests: 15% and 11%, respectively.

Vibration tests were performed in a LIND dynamic shaker and a rigid aluminum test plate, according to ESA specifications. Vibrations tests were performed on the samples in the three perpendicular axes; sine vibration from 5 to 10 Hz, and random vibration from 20 to 2000 Hz. All samples passed the vibration tests without noticeable changes in their optical power diffraction efficiency or response times.

4. Conclusion

A number of liquid crystal beam steering devices were manufactured, characterized and tested in a series of destructive and non-destructive tests in space-simulated conditions. All the manufactured devices passed the destructive tests according to ESA specifications with negligible or null damage in the cell structure, liquid crystal alignment, response times or 1st order diffraction efficiency. These passive liquid crystal devices are, therefore, appropriate for space applications,

withstanding the harsh environmental conditions of space missions, including launching and landing. Furthermore, it was determined that high quality glass does not suffer any sample darkening even after high radiation, and that PI alignment layers withstand both freezing and radiation without measurable damage.

Acknowledgment

References

[1] Z. Tang *et al.*, "Near-space flight of a correlated photon system," *Nature Sci. Rep.*, vol. 4, 2014, Art. ID. 6366.

[2] X. Shang *et al.*, "Electrically controllable liquid crystal component for efficient light steering," *IEEE Photon. J.*, vol. 7, no. 2, Apr. 2015, Art. ID. 2600113.

[3] E. Nowinowski-Kruszelnicki *et al.*, "Liquid crystal cell for space-borne laser rangefinder to space mission applications," *Opt. Electron. Rev.* vol. 20, no. 4, pp. 315–322, Dec. 2012.

[4] M. D. Watson and J. E. Pryor, "System engineering of photonic systems for space application," *Proc. SPIE*, vol. 9226, Nanophotonics and Macrophotonics for Space Environments VIII, 2014, Art. ID. 92260A.

[5] P. F. McManamon *et al.*, "A review of phased array steering for narrow-band electrooptical systems," *Proc. IEEE*, vol. 97, no. 6, pp. 1078–1096, Jun. 2009.

[6] V. Tkachenko *et al.*, "High accuracy optical characterization of anisotropic liquids by merging standard techniques," *Appl. Phys. Lett.* vol. 89, 2006, Art. ID. 221110.

[7] C. Falldorf, C. von Kopylow, and R. B. Bergmann, "Liquid crystal spatial light modulators in optical metrology," in *Proc. 9th Euro-Amer. WIO*, Helsinki, Finland, 2010, pp. 1–3.

[8] T. Kozacki, "Holographic display with tilted spatial light modulator," *Appl. Opt.*, vol. 50, no. 20, pp. 3579–3588, Jul. 2011.

[9] L. Li, D. Bryant, T. van Heugten, D. Duston, and P. J. Bos, "Near-diffraction-limited tunable liquid crystal lens with simplified design," *Opt. Eng.*, vol. 52, no. 3, 2013, Art. ID. 035007.

[10] J. Stockley and S. Serati, "Multi-access laser terminal using liquid crystal beam steering," in *Proc. IEEE Aerosp. Conf.*, 2005, vol. 1, pp. 1972–1977.

[11] J. Yan, Y. Li, and S. T. Wu, "High-efficiency and fast-response tunable phase grating using a blue phase liquid crystal," *Opt. Lett.*, vol. 36, no. 8, pp.1404–1406, 2011.

[12] L. Li, H. Yu, B. Y. Tang, and Z. Chen, "Wide steering-range motionless optical beam steering device, and methods of manufacture," U.S. Patent 7 146 070 B1, Dec. 5, 2006.

[13] S. Serati and J. Stockley, "Advances in liquid crystal based devices for wavefront control and beamsteering" in *Proc. SPIE*, 2005, vol. 5894, pp. 180–192.

[14] J. H. Park and I. C. Khoo, "Liquid crystal beam deflector with a photopolymer prism," *Mol. Cryst. Liq. Cryst.*, vol. 454, no. 1, pp. 135–143, 2006.

[15] N. Bennis *et al.*, "UV dichroism in vertically aligned nematic displays," *Mol. Cryst. Liq. Cryst.*, vol. 494, pp. 205–212, 2008.

[16] E. Otón *et al.*, "Dynamics and electrooptics of vertically aligned nematics with induced pretilt on SiOx," *J. Display Technol.*, vol. 6, no. 7, pp. 263–268, Jul. 2010.

[17] D. Cuypers, "*Vertically aligned nematic liquid crystal microdisplays for projection applications*," Ph.D. dissertation, Faculty Eng., Univ. Ghent, Ghent, Belgium, 2005.

[18] M. A. Geday *et al.*, "Development of liquid crystal based adaptive optical elements for space applications, in *Proc. ICSO*, Rhodes, Greece, 2010, pp. 1–4.

[19] M. A. Geday *et al.* "Automated characterization system for liquid crystal displays," *Proc. 6th IEEE Spanish Conf. Electron Devices*, Madrid, Spain 2007, pp. 318–320.